Cell Image Velocimetry (CIV): boosting the automated quantification of cell migration in wound healing assays

Supplementary Figures

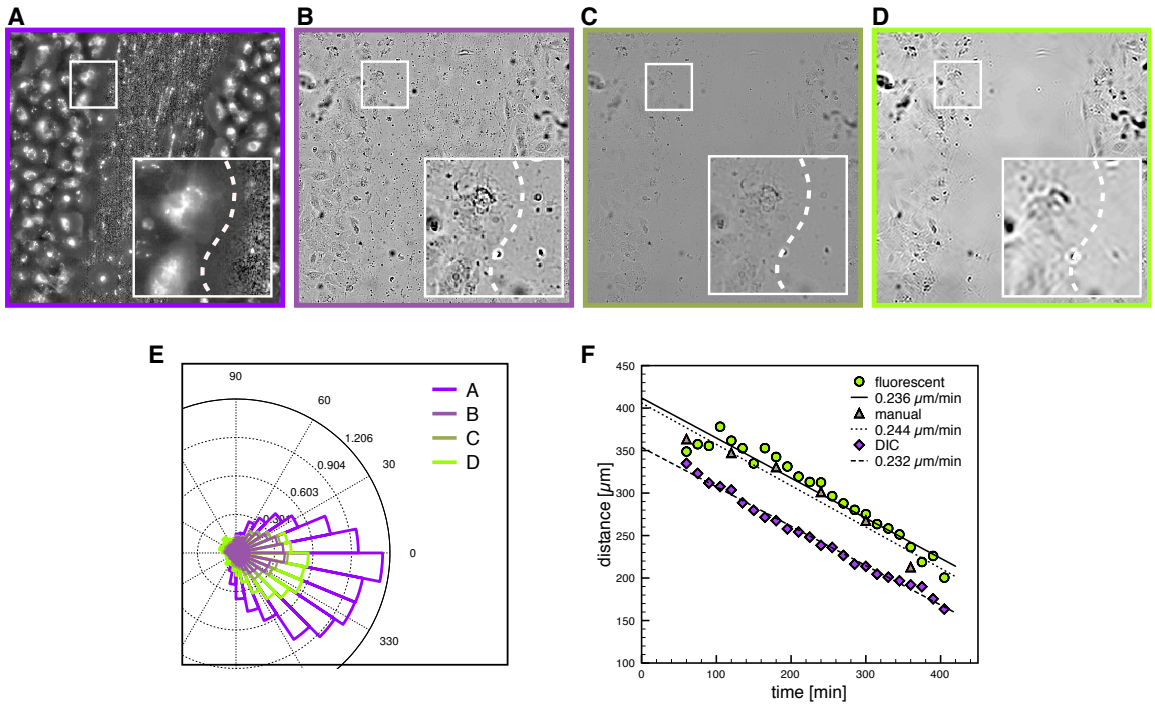

Fig. 1 Comparison of CIV analysis on fluorescent and corresponding DIC images. (A-D) Wound healing images. Box in lower left corner shows magnification of top left box. Dashed line indicates wound front. (A,B) Locally normalized fluorescent and DIC images (Eq. (1)). (C) Unfiltered DIC image. (D) Curvelet filtered DIC image. (E) Angular velocity distribution ($\mathscr{A}$) for PIV analysis of image datasets corresponding to A-D. (F) Comparison of wound distance for automated segmentation on fluorescent (green, circle) and DIC(purple, square) and manually segmented fluorescent (gray, triangle) images. Lines depict linear regression fits to the data.

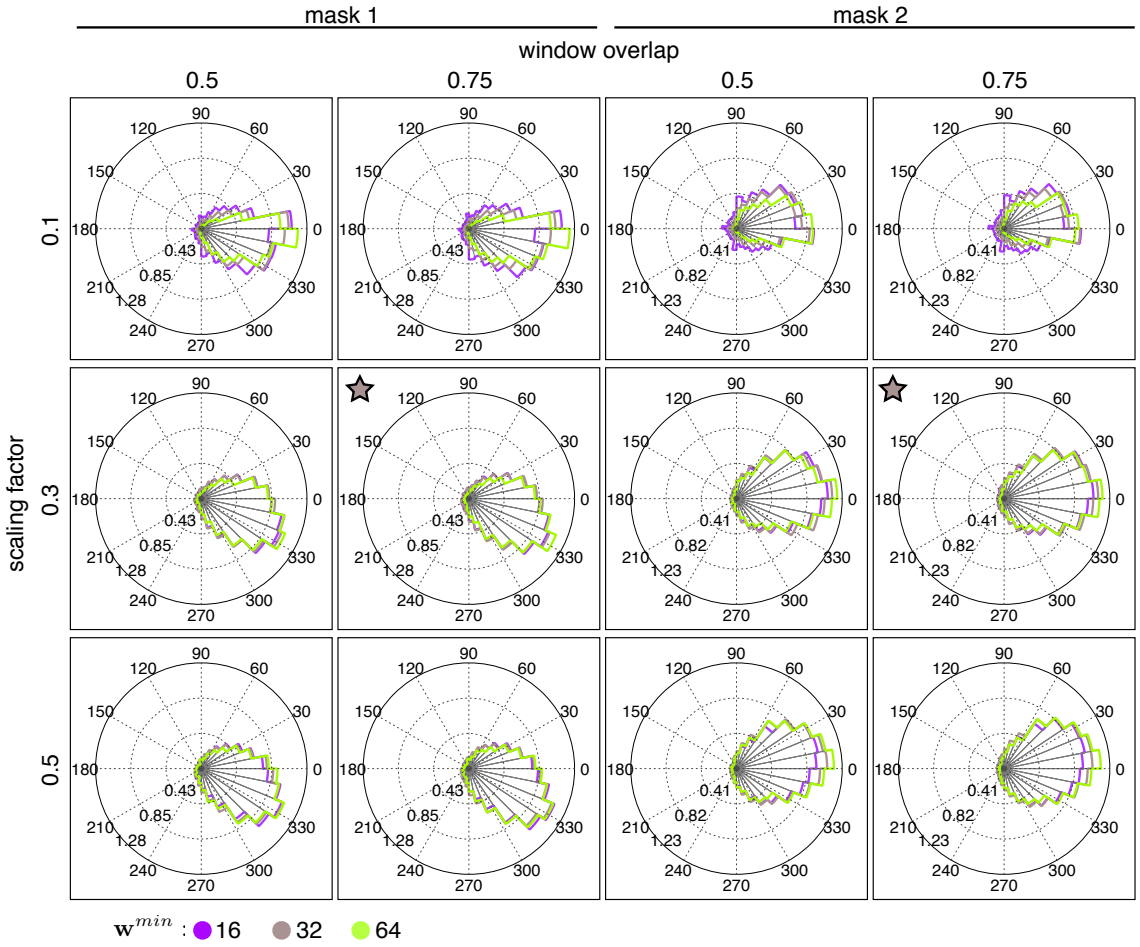

Fig. 2 Parametric study of PIV analysis parameter on the mean angular velocity distribution ($\mathscr{A}$) for the two disjoint cell layers (mask1, mask2) of a single experiment. Left to right: PIV sub-window overlap $ol_f = 50\%$ and 75%. Top to bottom: increasing scaling factor: $0.1, 0.3$ and 0.5. Color: minimal sub-window size $\mathbf{w}^{min} = 16, 32$ and 64 pixels. Stars indicate the default parameter sets used in this study.

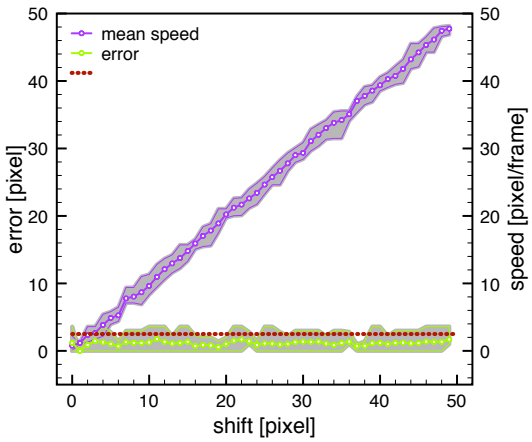

Fig. 3 Assessment of the shift correction algorithm on artificially introduced shifts in consecutive image frames. Green: mean error in the difference of the detected shift and the introduced shift (left y-axis). Purple: mean speed detected in the velocity field V (right y-axis). Red: threshold value in mean speed for shift correction (2.5 pixel/frame). Connected dots represent mean values, lines outlining the colored areas mark observed minima and maxima.

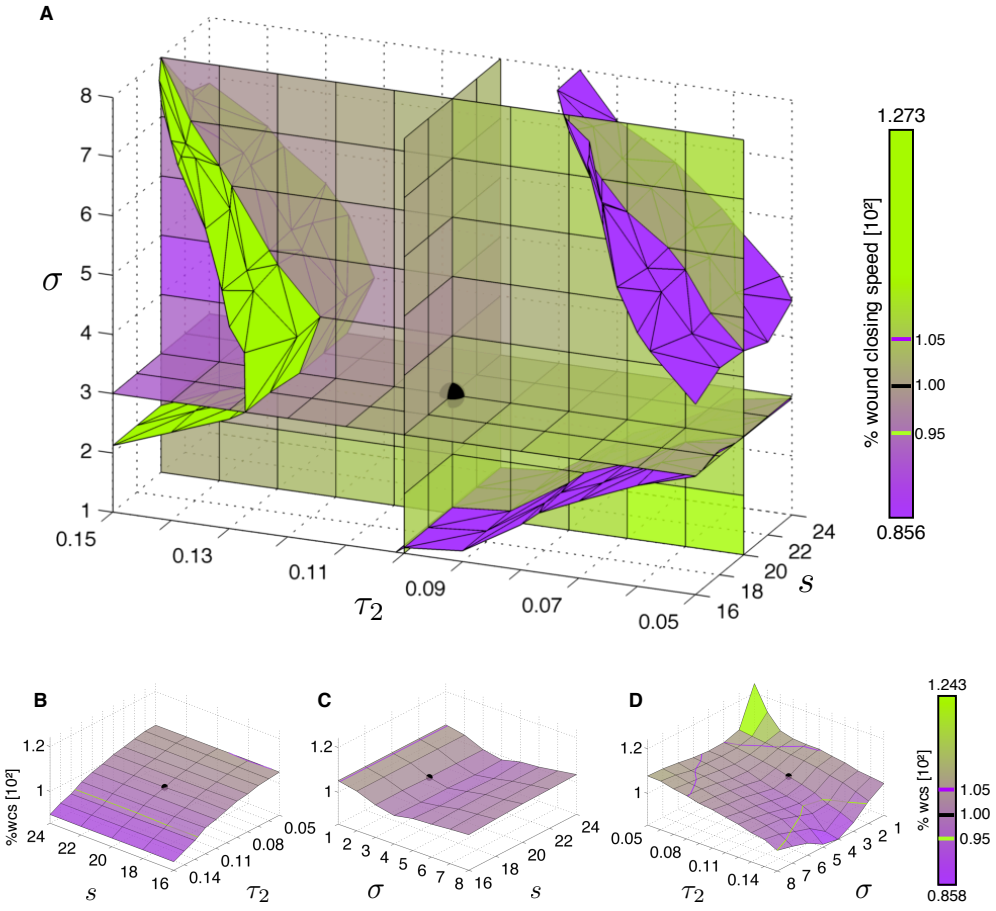

Fig. 4 Parametric study on cell layer segmentation algorithm for parameters: LoG filter size (s), LoG standard deviation (σ) and the difference image threshold (τ_2). Black dot indicates reference parameter set used for quantification. (A) Quantification of observed wound closing speed (wcs) for varying s, σ and τ_2 in percentage to wcs of reference solution. Slices depict variations in observed wcs for constant s σ and τ_2 respectively. Green and purple planes indicate $\pm 5\%$ error-isoplanes. (B-D) Surface plots for individual slices shown in (A). Green and purple lines indicate $\pm 5\%$ error-isobars.

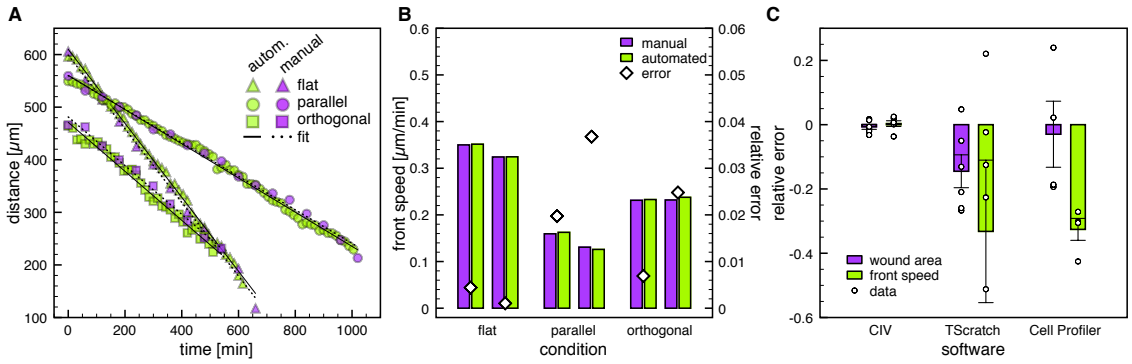

Fig. 5 Comparison of automated cell layer detection versus manual cell layer segmentation and available wound healing analysis software TScratch[5] and Cell Profiler[39]. (A,B) Green: automated analysis data. Purple: manually generated data. (A) Comparison of estimated wound distance for three experiments (circles: flat substrate, triangles: parallel gratings and boxes: orthogonal gratings). Symbols represent data points. Solid lines depict linear regression fits to the automated data, solid lines represent the corresponding fits to the manually segmented data. (B) Comparison of estimated cell layer front speed for automated and hand segmented data (bar plot, left y-scale). Diamonds depict the detected error of the automatically detected front speed with respect to the manually detected value (right scale). (C) Comparison of detected wound area (purple) and wound closing speed (green) by available software packages compared to manual segmentation results.

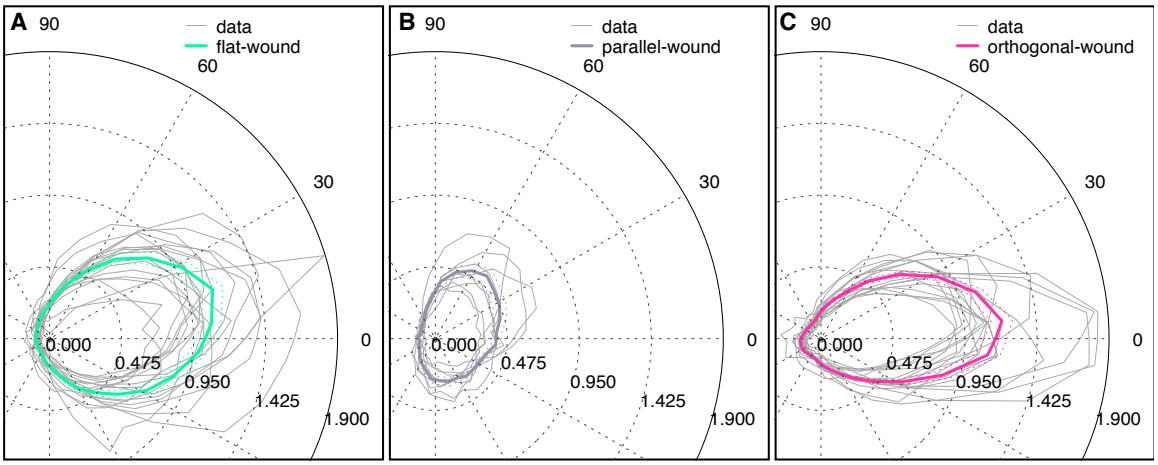

Fig. 6 Mean angular velocity estimation on a flat substrate (A, n=18), in the presence of parallel (B, n=8) and orthogonal gratings (C, n=18). Gray lines show deflected $\mathscr{A}$ distributions of individual experiments. Solid colored lines show mean values, dashed colored lines represent standard error of mean.

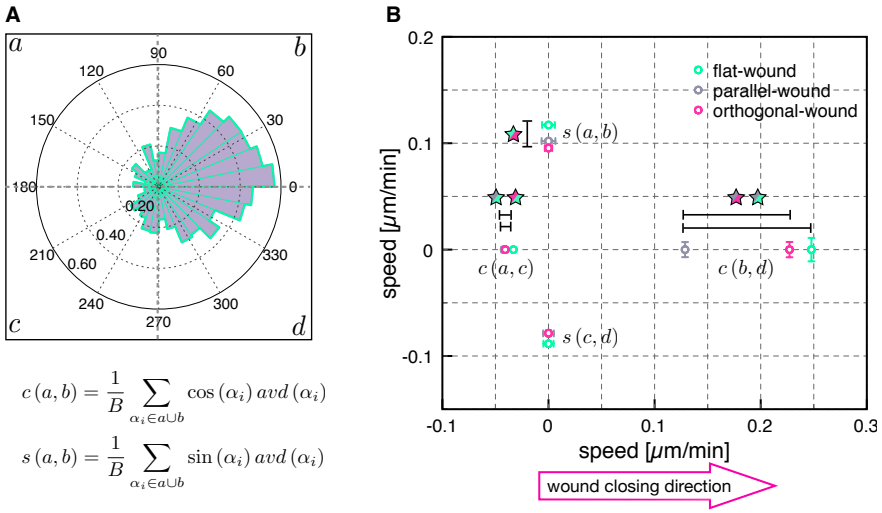

$$c(a,b) = \frac{1}{B} \sum_{\alpha_i \in a \cup b} \cos(\alpha_i)\, avd(\alpha_i)$$

$$s(a,b) = \frac{1}{B} \sum_{\alpha_i \in a \cup b} \sin(\alpha_i)\, avd(\alpha_i)$$

Fig. 7 In axis velocity contributions of angular velocity distribution. (A) Conceptual sketch of the $\mathscr{A}$ components considered for the axial contributions (top) and the formula to calculate the axial contributions (bottom) with B, the number of angular bins (see Eq. (**??**)). (B) Axial contributions of the $\mathscr{A}$ distribution. Turquoise: flat substrate (n=18), purple: parallel topography (n=8), pink: orthogonal topography (n=18). Error bars represent standard error of mean. Colored stars and black bars indicate significance ($p < 0.05$, Wilcoxon rank-sum test) with respect to the experiment of the according colors.

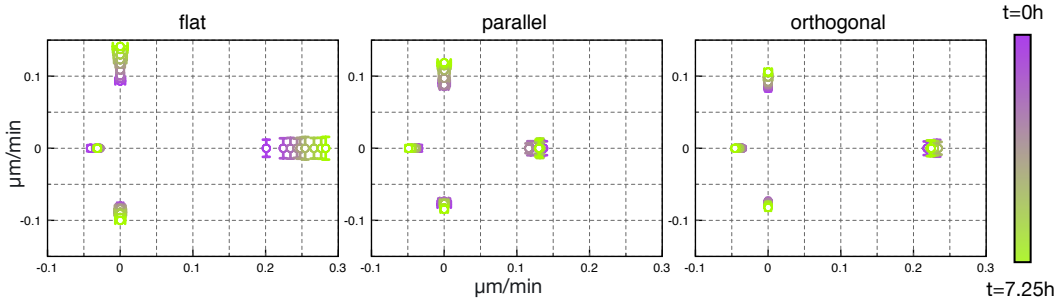

Fig. 8 Temporal evolution of the axial contributions of the $\mathscr{A}$ distribution. Left to right: flat substrate (n=18), parallel topography (n=8) and orthogonal topography (n=18). Color indicates temporal progression.

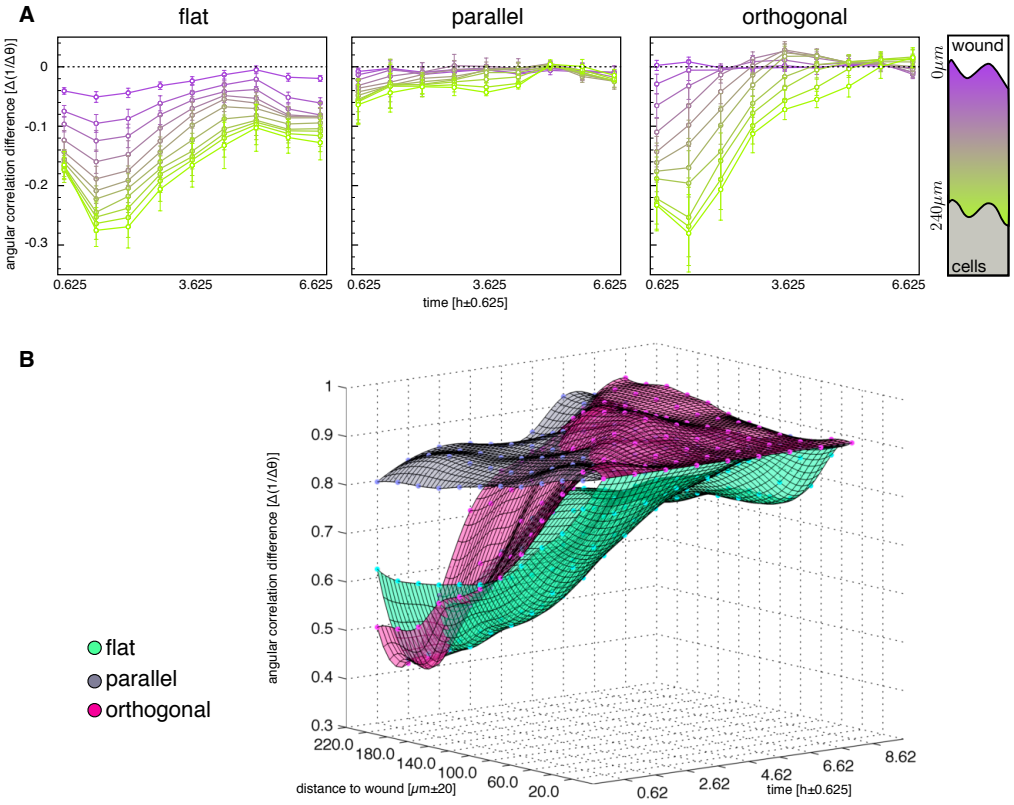

Fig. 9 Spatiotemporal evolution of the difference in angular correlation with respect to the front layer of cells. Temporal and spatial binning corresponds to the description given in Fig. 5. (A) Color represents the distance to the wound. Error bars show standard error of mean. (B) Collapsed surface plot of data depicted in (A). Colors denote experimental conditions: Turquoise: flat substrate, purple: parallel topography, pink: orthogonal topography. Colored dots depict mean values, surface represents a B-spline fit to the data points. Sample sizes vary for bins: flat substrate ($10 \leq n \leq 12$), parallel topography (n=4) and orthogonal topography ($8 \leq n \leq 12$).